International Journal of
INTELLIGENT SYSTEMS AND APPLICATIONS IN ENGINEERING
ISSN:2147-6799 www.ijisae.org Original Research Paper

Control Strategy for Rotor-Side Converter (RSC) and Grid-Side Converter (GSC) in a Grid-Interfaced Wind-DFIG Based System

Rana Adil Abdul-Nabe[1], Mihaela Constantin [2], Cătălina Dobre [3], Gabriel Fischer-Szava [4], Georgiana Dăescu (Duiculete)[5], Nicolae Băran[6], Sevastiana Areta Ghioca[7]

Submitted: 05/09/2024 **Revised:** 22/10/2024 **Accepted:** 01/11/2024

Abstract: Wind energy conversion systems (WECS) are a significant and rapidly increasing contributor to the generation of electrical power in the new era of power production systems. They have the potential to significantly enhance the power supply situation in communities situated in remote regions. Wind energy conversion systems (WECS) are a substantial and ever-growing contributor to the production of electrical power. In this paper, a novel method for synchronizing DFIG grid connections in wind-generating systems that operate at varying velocities is introduced. The utilization of stat flux-oriented vector control for the back-to-back PWM converters simplifies the synchronization process in the DFIG rotor circuit. The electromotive force (EMF) of the stator can be adjusted to align with the grid voltage by regulating the rotor d-axis current. In order to rectify any potential phase shift that may arise between the voltage of the grid and the electromagnetic field of the stator, implement the phase-locked loop (PLL) circuit. The generator's speed is determined by the turbine pitch angle, while the frequency of the stator is regulated to ensure that it is in harmony with the grid's frequency. the proposed methodology simulation tests using the Matlab/Simulink toolbox to validate the proposed synchronization algorithm, showcasing its effectiveness in facilitating the seamless integration of the DFIG into the grid for wind power generation applications.

Keywords- *DFIG, RSC, GSC, Grid Integration, Power Flow Control, Battery*

1. Introduction

Global warming and the depletion of fossil fuels are major concerns for the climate. Green energy sources have become a new way for people to get the energy they need. In the past few years, there has been a lot of interest in making electricity from oceans, waves, geothermal energy, solar energy, and wind energy. In the future, Wind power will be very important in the energy industry.The rapid growth of wind power technology demonstrates that it is gaining global attention [1]. DFIGs are useful in current energy systems because they can work at different speeds and handle both active and reactive power. In DFIG, we connect the stator directly to the power grid. For the rotor, we use a bi-directional converter to manage the active and reactive power exchanged between the stator and the AC supply network [2]. According to wind turbine technology, the rotor current disrupts the vector control method, which comprises active and reactive power components. Rotor current drivers control these parts by altering the direction of the rotor current excitation voltage [3, 4]. We must try to solve the problems necessary for the operation of large-scale wind farms. We used the electromechanical model to connect the DFIG and wind blades, thereby creating a nonlinear feedback controller. The world needs to use more renewable energy because traditional power plants aren't sustainable and are detrimental for the earth [5, 6]. Some of the technical issues that arise when using electric power systems include power quality, dependability, and safety. A lot of people are interested in wind energy because it is a green energy source that is also cheaper than other power sources. Wind energy undergoes constant changes due to significant fluctuations in natural wind patterns. The wind energy conversion method faces numerous challenges as its energy fluctuates significantly more than that of other energy sources [7-9]. When the power goes up and down, the frequency changes, which makes the highly penetrated unstable system. It's not a straight

ranaalbakri2018@gmail.com 1 ,
i.mihaelaconstantin@gmail.com2
catalina.dobre@upb.ro 3 ,
fischer_gabriel2002@yahoo.com 4 ,
georgiana.duiculete@gmail.com 5 ,
n_baran_fimm@yahoo.com 6 ,
sevastianaghioca@yahoo.ro7
Department of Thermotechnics, Engines, Thermal and Refrigeration Equipment, National University of Science and Technology Polytechnic , 060042, Bucharest, Romania.

line between the stator current and the rotor current. The rotor current controller requires careful tuning to ensure stability and sufficient transient reactions within the operating range [12–14]. In addition, the field-oriented control needs to guess or measure the flow. Adjustments to the output of generating units are necessary to satisfy the demands for both active and reactive power [15].

These kinds of moves must have as low an upkeep cost per unit as possible, and the network must have enough wind generators to handle AC disturbances from the outside. A more sophisticated control system proposed limiting the generator's over current by monitoring the network fault in the event of unbalanced voltage. This effectively reduces the voltage network disturbance [16, 17]. To address the relay security issues in a power grid with Doubly Fed Induction Generators (DFIGs), it is necessary to study how fault currents behave in DFIGs. These conditions are not the same as those of a normal synchronous generator. The fault current characteristics of DFIG (transient components and damping time constants) differ under the conditions examined. So, it's important to look at DFIG's features separately for certain situations [18, 19]. Numerous studies have proposed solutions for fault situations. However, determining the fault current characteristics of the DFIG can be challenging due to the dynamic response of the AC/DC/AC converter during a fault. We studied the DFIG fault current under the assumption that the excitement current would remain constant before and after the fault [20, 21]. A study based on the above premise is useless for real-world systems. Since then, considerable research has examined fault current features and how the rotor-side converters RSC and GSC react to load variations. That research doesn't meet the security study's needs. To cover this gap, we propose a theoretical analytical method for DFIG fault current characteristics under normal conditions. The agitation of the rotor windings greatly influences the stator fault current, necessitating the connection of the wind machines to maintain system stability during and after a malfunction. Doing things this way may worsen systemic behaviors. If we analyze transients [22, 23], we can isolate the field disturbance from turbine engine activity. The rotor-side converter's capacity can boost the stator's performance. The DC link voltage and fault current are utilized to meet the needs of the DFIG during voltage drops. The analysis revealed that removing the study's commotion improved the DFIG's transient behavior. We employed dynamic model analysis in the nonlinear control design to identify the instability and improve generator performance.

This study shows a complete way to control both the rotor-side converter (RSC) and the grid-side converter (GSC) in a DFIG-based wind energy system that is connected to the power grid. The text describes the process of modeling the Doubly Fed Induction Generator (DFIG) using space vector theory. This entails the transformation of the three-phase windings into stationary and revolving reference frames. The dq frame vector control approach is recommended for the efficient separation of the d and q values, which allows the DFIG to operate in a manner similar to that of a DC motor. Consequently, the precision and efficacy of control are improved. Furthermore, the paper discusses the three operating phases of the DFIG sub-synchronous, hyper-synchronous, and synchronous in accordance with the angular velocities of the rotor and stator. This control approach guarantees the optimal flow of power and stability in the grid-interfaced wind energy system, thereby enhancing reliability and performance.

2.Theoretical study

The Mohammad Nasir Uddin and associates (2023) have proposed a neurofuzzy-based adaptive direct power control (DPC) strategy for a grid-linked DFIG-based WECS. The method provides low-voltage ride-through (LVRT) capabilities and is capable of managing grid-side disturbances through the use of rotor-side converter management. The ANFIS-DPC scheme has been shown to exhibit superior dynamic performance in comparison to conventional PI controllers. In order to defend the WECS from grid faults and unexpected wind speed fluctuations, we implemented the proposed distance protection and DPC strategies in a laboratory environment.

In 2023, the Souvik Das and Bhim Singh We introduce a neurofuzzy-based adaptive direct power control (DPC) scheme for a grid-linked DFIG-based WECS. This method employs the normalized maximum correntropy criteria (NMCC) to mitigate the voltage distortions and power fluctuations that are the result of unbalanced loads in the grid environment. Furthermore, the method is parametrically robust, which eliminates the necessity for intricate regulators and ensures that DFIG rotor currents are distortion-free, even when applied at voltages that are not optimal. The scientific findings of the experiments served as evidence of the efficacy of the NMCC-based control method. In order to ensure that a TCSC-compensated TL that is connected to a DFIG-installed wind farm is safeguarded in a timely and reliable manner, it is necessary to implement enhanced defect detection and classification methods for distance relays, as per author Alberto Berrueta et al. (2023).

In WECS, Subodh Kumar Mohanty et al. (2024) introduce a direct torque and flux control technique for grid-connected DFIG management. It uses an adaptive ANFIS to optimize dynamic performance. The technique generates PWM switching signals by

comparing the actual torque and stator flux with the references. We recommend a hybrid training algorithm to account for the uncertainties associated with wind speed and WECS nonlinearities. Mohammed Alqahtaniet al. (2023) this paper aims to accurately simulate a type-3 wind turbine using a DFIG under grid imbalance. We transform the steady-state analysis problem into an optimization problem and include a positive sequence component and a third harmonic circuit in the study. The steady-state analysis creates phasors with harmonic parts, and a nonlinear optimization tool solves the optimization problem.The paper enhances the efficiency of steady-state analysis computation by employing a sophisticated phasor model of DFIG and advanced solvers.

23. Modeling's

3.1 Wind modelling

Wind turbine modeling focuses on converting kinetic energy from the wind into mechanical energy, primarily through aerodynamic forces. Due to the stochastic nature of wind speed, turbines do not consistently operate at their rated capacity but can achieve this at rated wind speeds (e.g., 12 m/s). The aerodynamic power generated by a wind turbine is known by:

$$P_w = \frac{1}{2}\rho\pi R^2 v_w^3 \qquad \text{Eq.1}$$

Where ρ is air density, RRR is the blade radius, and v_w is wind velocity (Ullah et al., 2017). The mechanical power P_t is represented as:

$$P_t = \frac{1}{2} Cp\ (\lambda,\beta)\rho\pi R^2 v_w^3 \qquad \text{Eq.2}$$

Here, Cp is the coefficient of performance, λ is the tip speed ratio (TSR), and β is the blade pitch angle (Sami et al., 2020). The TSR is defined as:

$$\lambda = \frac{\Omega_t \times R}{V_W} \qquad \text{Eq.3}$$

Where Ω_t is the angular shaft speed of the turbine (Sami et al., 2020). The relationship between Cp and λ is expressed as:

$$Cp = c_1\left(\frac{C_2}{\lambda} - 1\right)e^{-c3/\lambda} \qquad \text{Eq.4}$$

with c_1, c_2, c_3, being positive constants (Ullah et al., 2017). Maximum power extraction occurs when $\lambda = \lambda_{opt}$ and $Cp = Cp{-}max$ The induced torque is given by:

Where G is the gear ratio, Tr is generator torque, and Tt is aerodynamic torque (Ebrahimkhani, 2016). By substituting the torque expression into the mechanical power equation, the reference generator speed can be derived:

$$\Omega r{-}ref = \left(\lambda opt \times \frac{G}{R}\right)v_w \qquad \text{Eq.5}$$

3.2 DFIG Modeling

The stator and rotor are equipped with windings that comprise the DFIG. It features rings that are easily attached. The stator has three-phase protected windings that are linked to the grid by a three-phase transformer. This is also true for the rotor, which is made up of protected three-phase windings. The rotor windings are linked to an outside fixed circuit by a set of moving rings and brushes. There are parts like these that let the control rotor current flow into or out of the rotor windings. This is how the dynamic model of the DFIG is shown: with direct and indirect transformations. Space vector theory lets us show that the three windings of the rotor and stator can be broken down into two windings that are stationary for the stator and one winding that is spinning for the rotor. Space vector theory lets us show how the DFIG works by changing the three-phase windings of the stator and rotor into two-phase systems. The rotor windings are shown by moving dq coordinates, while the stator windings are shown by fixed α^2 coordinates. This is how you write the voltage vector for the stator and rotor: showing in fig.1

Stator and Rotor Voltage Vector Equations:

The stator voltage vector in the dq frame is expressed as:

$$\overrightarrow{u_s} = u_{ds} = R_s i_{ds} + \frac{d_{\psi ds}}{dt} - \omega_s \psi_{qs} \qquad \text{Eq.6}$$

$$\overrightarrow{u_s} = \begin{cases} u_{ds} = R_s i_{ds} + \frac{d_{\psi ds}}{dt} - \omega_s \psi_{qs} \\ u_{qs} = R_s i_{qs} + \frac{d_{\psi qs}}{dt} - \omega_s \psi_{ds} \end{cases}$$

The rotor voltage vector in the dq frame is expressed as:

$$\overrightarrow{u_r} = \begin{cases} u_{dr} = R_r i_{dr} + \frac{d_{\psi dr}}{dt} - \omega_r \psi_{qr} \\ u_{qr} = R_r i_{qr} + \frac{d_{\psi qr}}{dt} - \omega_r \psi_{dr} \end{cases}$$

Where:

- u_{ds}, u_{qs} , $u_{d,r}, u_{qr}$ the voltages of the stator and rotor in the dq reference frame
- i_{ds} , i_{qs} , i_{dr}, i_{qr} stator and rotor currents in the dq reference frame, respectively.
- Rs,Rr: stator and rotor resistance values, respectively.
- ω_s,ω_r: stator and rotor angular speeds, respectively.

Operating Modes of DFIG

The operating modes of the DFIG are determined by the relative speeds of the stator and rotor, defined as follows:

$\omega_s = \omega_r + \omega_m$

$s = \frac{\omega s - \omega m}{\omega s}$

Where:

- ω_s: Synchronous speed.
- ω_r: Rotor speed.
- ω_m: Mechanical speed.
- s: Slip.

Based on the speed relationship, the DFIG can operate in three modes:

Sub-Synchronous Operation ($\omega_m < \omega_s$)

$\omega_s > 0$

$s > 0$

Hyper-Synchronous Operation ($\omega_m > \omega_s$)

$\omega r < 0$

$s < 0$

Synchronous Operation ($\omega_m = \omega_s$)

$\omega_r = 0$

$s = 0$

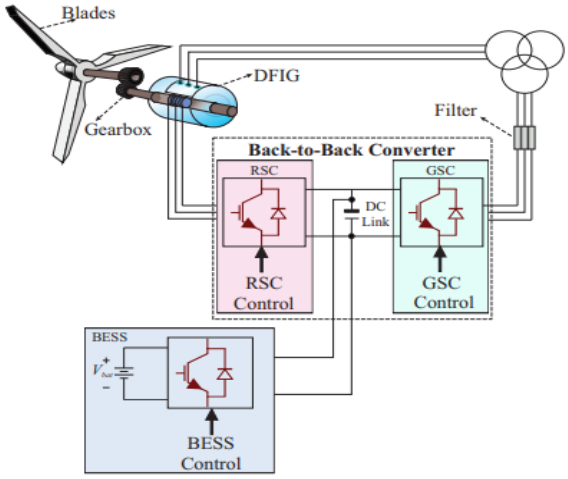

Figure 1.DFIG wind system with BESS

The stator flux vector is aligned with the d-axis component showing in the fig.2

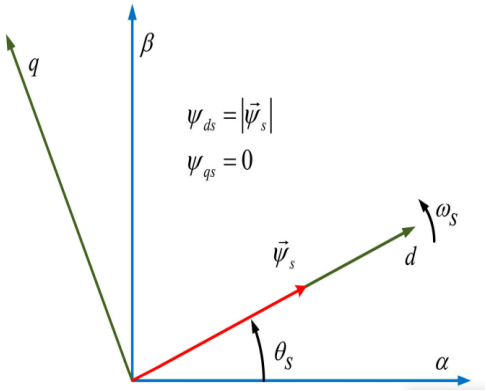

Figure 2. The stator flow vector is pointing in the direction of the d-axis.

Grid-side control Figure 3 illustrates the system configuration, which includes the grid voltage, filter, and GSC. The power supply of the DFIG is regulated using the GSC control strategy.

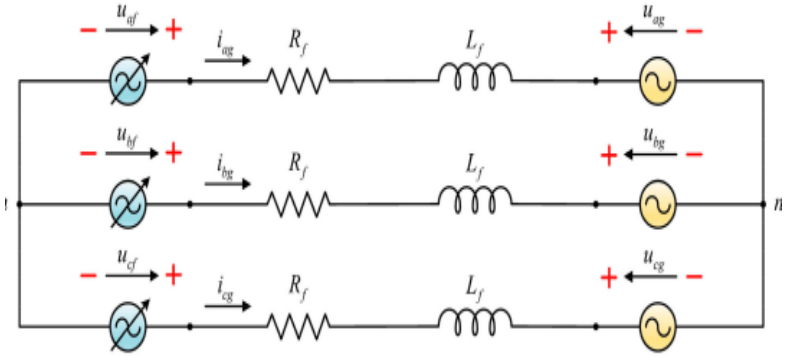

Figure 3. A simplified illustration of the three-phase grid system.

The DC connection voltage (Vbus) and the reactive power (Qg) exchange with the grid are two important things to think about when controlling the flow of power. The dq model for the grid side system is shown in Figure 4 in a frame that stays still. Equation (24), shown in Figure 5, shows the straight part of the voltage vector that is oriented along the

ωs. Equation (25) can be used to show the dq part of the filter voltage.

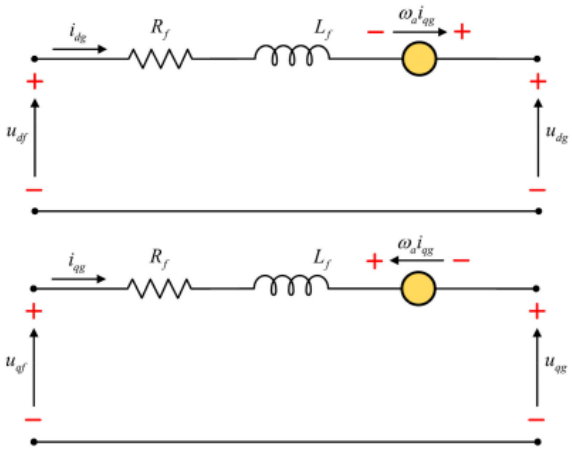

Figure 4 the grid-side system's dq model in the fixed frame is shown in a simplified form.

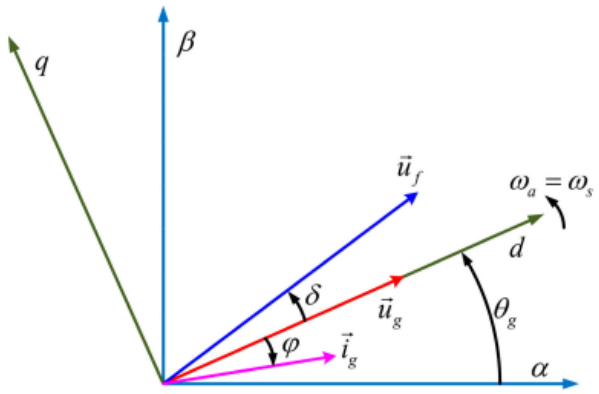

Figure 5. Vector of grid voltage orientated with ωs.

3.3 Control Strategy for RSC and GSC in DFIG

The intention of the control strategy for the RSC and GSC in a DFIG is to guarantee the correct operation and regulation of active and reactive power flow. To decouple the control of active and reactive power, this strategy employs a vector control approach, as illustrated in the dq frame.

Control Strategy

The grid-side voltage and the associated equations are given as:

$$\begin{cases} u_{dg} =\rightarrow u_g \\ u_{qg} = 0 \\ \omega_a = \omega_s \\ \theta = \omega_{at} \implies \theta = \theta_g \ \omega_s t \end{cases}$$

The voltages in the dq frame for the GSC are expressed as:

$$\begin{cases} u_{df} = R_f i_{dg} + L_f \frac{d i_{dg}}{dt} - \omega_s L_f i_{qg} \\ u_{qf} = R_f i_{qg} + L_f \frac{d i_{dq}}{dt} - \omega_s L_f i_{dg} \end{cases}$$

The active power (Pg) and reactive power (Qg) exchanged with the grid are given by:

$$\begin{cases} P_g = \frac{3}{2} u_{dg} idg + u_{qg} iqg \implies Pg = \frac{3}{2} u_{dg} idg \\ Q_g = \frac{3}{2} u_{qg} idg - u_{dg} iqg \implies Qg = -\frac{3}{2} u_{qg} idg \end{cases}$$

International Journal of
INTELLIGENT SYSTEMS AND APPLICATIONS IN ENGINEERING
ISSN:2147-6799 www.ijisae.org Original Research Paper

From Equation (26), we can see that the idgcurrent component controls the active power (Pg), while the iqg current component controls the reactive power (Qg).

3.4 BESS modelling

Depending on the particular requirements of the system and the current technology, DFIG-based WECS might also use other energy storage methods. Because of its high power density and fast response time, the BESS is especially well-suited for uses requiring a high power output and fast load response, including wind energy systems. Its main advantage is this. Because of its extended life cycle and capacity to run in hostile conditions, this consistent and durable choice for energy storage in wind energy systems is perfect. As such, many writers choose to use a BES instead of another kind of energy storage system. The features of different ESS devices are defined in [21].This model considers the steady-state performance of the device by means of an analysis of the total power transfers across a battery bank and modulates the SOC across the designated time span [22,23,24]. This approach ignores elements including temperature changes, lifetime deterioration, capacity fluctuations dependent on operational voltage, and individual electrical circuits [25,26,27]. The battery model obtains the intended 1PSET (defined in units of nominal capacity) from its regulating model by updating the SOC of the battery. Figure 10 shows Bess model parameters. Equations (22) and (23) with regard to generator conventions define the computation of the real power, 1PB, either supplied into or from the battery.

$$\Delta \boldsymbol{PB}=\boldsymbol{\eta_{CHARGE}}\Delta \boldsymbol{P_{SET}},\Delta \boldsymbol{P_{SET}}<\boldsymbol{0}$$

$$\boldsymbol{PB}= \frac{\Delta \text{PSET}}{\eta \text{discharge}} \quad \Delta \boldsymbol{P_{SET}}\geq \boldsymbol{0}$$

The discharge and charge efficiencies of the Bess are correspondingly where $\boldsymbol{\eta DISCHARGE}$. It should be mentioned that the BESS produces a result expressed in Δ. This suggests that some of the BESS's available capacity might be used for other purposes, such buffering or energy storage. Showing in Figure 6

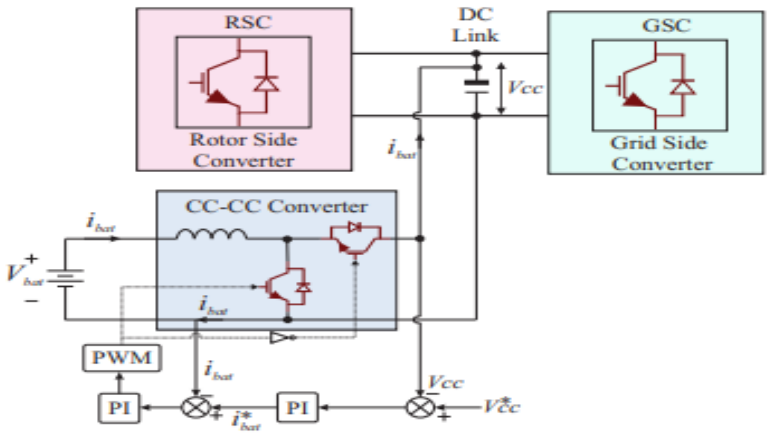

Figure 6. BESS Control Diagram

3.5 Grid Synchronization and Connection

The converters are unable to be connected to the grid, and their output signals cannot be synchronized with the grid's frequency, unless the angle of the grid voltage is known. A Phase Locked Loop (PLL) is one method of achieving this synchronization. The converter voltages and currents endure coordinate transformations as a result of changes in the grid phase voltages, as illustrated in Figures 8. The PLL output must be corresponding to the angle in order to complete these modifications. The PLL and a filter are together necessary for connecting the converters to the grid. The GSC filter is visible in Figure 7. It is accountable for the connection of the grid voltage to every phase of the converter's output.

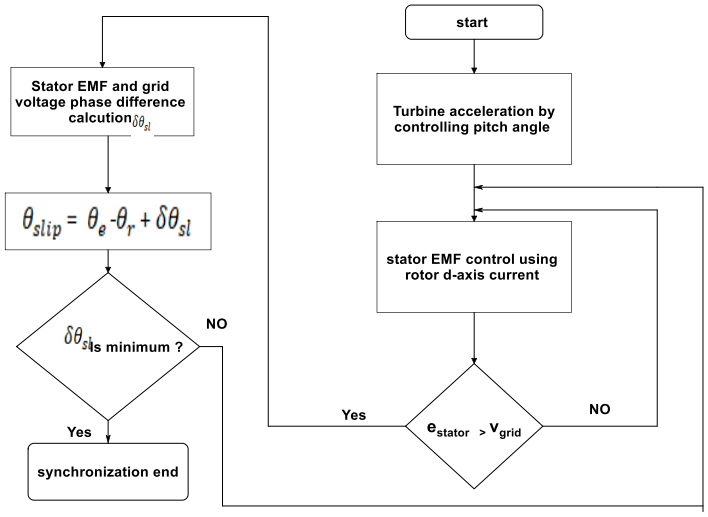

Figure.7 Grid Synchronization and Connection

4.Proposed Approach

The proposed methodology of this paper to improved wind energy conversion system efficiency and dependability. It is integrated with DFIG, BESS, GSC, and RSC modules. The method with integrated modules involved simulating a DFIG system with a BESS and other subsystems on MATLAB software. The wind-based DFIG is the main renewable energy source of the system, and the BESS serves as an additional energy storage option to improve the stability and flexibility of the system. The battery, which acts as the system's input, stores the renewable wind energy that the DFIG harvests. The Simulink model employs a bidirectional DC-to-DC converter to charge and discharge the battery system, ensuring seamless operation with the DFIG system. The control algorithms RSC and GSC that modify the DFIG, battery converter, and grid connection all contribute considerably to the system's overall performance. The main parts of the DFIG system is GSC and the RSC this is adapting the flow of energy between the DFIG and the grid system, the GSC makes sure that operations are dependable and stable while upholding grid standards. Though, in order to maximize wind energy extraction and attain a Unity Power Factor (UPF), the RSC is responsible for operating the DFIG. By adding the BESS to the DC connection between the two back-to-back voltage source converters (VSCs), the system's overall performance is improved, and its energy storage capacity is increased. The Fuzzy Proportional Integral Derivative (FOPID) controller controls the BESS and converters, ensuring effective and continuous power transfer throughout the system. This strategy, which combines energy storage with renewable energy generation, provides a workable substitute for improving the efficiency and dependability of wind energy conversion systems.

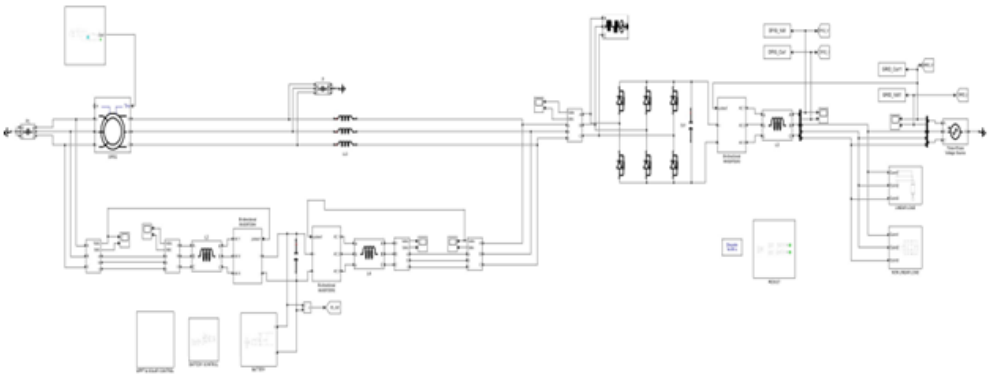

Figure 8 Proposed Simulink Model

4.1 Mathematical Modelling of Proposed System

Analyze the mathematical of the proposed system here showing the DFIG modelling with battery

DFIG: The following equations help one to define the dynamic equations of a DFIG: Stator equations:

$v_{ds}=Rs_ids-\omega_e\lambda_{qs}+d_\lambda ds/dt$ Eq.7

$vqs=R_{si}q_s+\omega_e\lambda ds+d_{\lambda q}s/dt$ Eq.8

Rotor equations:

$v_{dr} = Rridr+\omega_s\lambda_{qr}+d_{\lambda d}r/dt$ Eq.9

$v_{qr} = Rriqr-\omega_s\lambda_{dr}+d_{\lambda q}r/dt$ Eq.10

Electromagnetic torque:

$Te=(3/2)P(\lambda_d s_i qr-\lambda_q s_i dr)$ Eq.11

Where:

v_{ds},v_{qs}: Stator voltage components in the synchronous reference frame.

v_{dr},v_{qr}: Rotor voltage components in the synchronous reference frame.

i_{ds},i_{qs}: Stator current components in the synchronous reference frame.

i_{dr},iqr: Rotor current components in the synchronous reference frame.

$R_{s,}R_r$: Stator and rotor resistance, respectively.

ω_e: Electrical angular velocity.

ω_s: Mechanical angular velocity.

λ_{ds},λ_{qs}: Stator flux linkages.

λ_{dr},λ_{qr}: Rotor flux linkages.

P: Number of pole pairs.

BESS: The behavior of the battery can be modeled using an equivalent circuit model, which includes parameters such as internal resistance, voltage, and state of charge (SoC). The battery dynamics can be described using:

Battery voltage:

$Vb=Voc(SoC)-I_bR_{int}$ Eq.12

Battery current:

$I_b=Ic_h-I_{dis}$ Eq.13

Where:

V_b: Battery voltage.

Voc(SoC): Open circuit voltage as a function of State of Charge.

I_b: Battery current.

I_{ch},I_{dis}: Charging and discharging current, respectively.

R_{int} : Internal resistance of the battery.

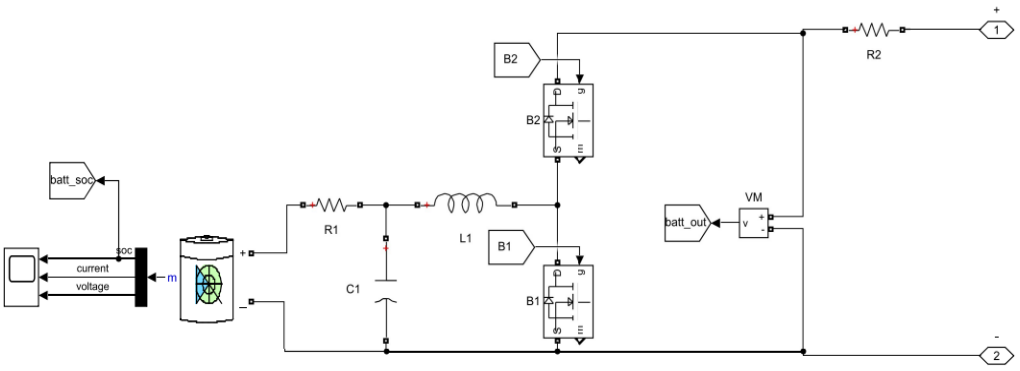

Figure 9: Battery Simulink Model

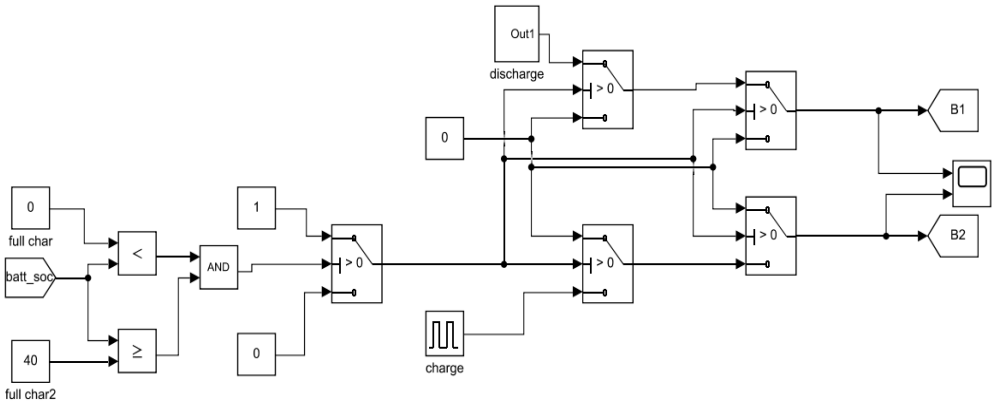

Figure 10: Battery Control

GSC: Managing the grid's active and reactive power flows is the primary control purpose of the GSC. The control strategy typically involves a PI controller for active power control and a PI controller or a FOPID controller for reactive power control. The control equations for the GSC can be expressed as follows:

Active power control:

$P_{ref}=P_{setpoint}-P_{actual}$

$Vd\_ref=Vd\_ref\_0+K_p(Pref)+K_i\int P_{ref}dt+K_d \cdot Pref/dt$ Eq.14

$Vq\_ref=0$

Reactive power control:

$Q_{ref}=Q_{setpoint}-Q_{actual}$

$V_{q\_ref}=V_{q\_ref}\_0+K_p\_q(Q_{ref})+K_i\_q\int Q_{ref}\,dt+K_{d\_q} \cdot dQ_{ref}/dt$ Eq.15

$V_{d\_ref}=0$

Where:

P_{ref}: Active power reference.

$P_{setpoint}$: Desired active power setpoint.

P_{actual}: Actual active power.

V_{d_ref}, V_{q_ref}: Reference d-axis and q-axis voltages.

$V_{d\_ref}\_0$, Vq_ref_0: Initial reference voltage values.

Q_{ref}: Reactive power reference.

$Q_{setpoint}$: Desired reactive power setpoint.

Q_{actual}: Actual reactive power.

K_p, K_i, K_d: Proportional, integral, and derivative gains for active power control.

K_{p_q}, Ki_q, K_{d_q}: Proportional, integral, and derivative gains for reactive power control.

Rotor Side Converter (RSC): The control objective of the RSC is to control the rotor currents to achieve unity power factor and optimize the energy extraction from the wind. The control equations for the RSC can be expressed as follows:

Unity Power Factor Control:

$I_{qr\_ref} = -$ Vds/ Xr

$I_{dr\_ref} =$ Vqs/ Xr

Where:

I_{qr_ref}: Reference q-axis rotor current.

$I_{dr\_ref:}$ Reference d-axis rotor current.

V_{ds}: Stator d-axis voltage.

V_{qs}: Stator q-axis voltage.

$X_{r:}$ Rotor reactance.

FOPID Controller for Reactive Power Control in GSC: The FOPID controller enhances the classic PID controller by incorporating fractional order characteristics, resulting in increased adaptability and robustness. The control system is designed to regulate the flow of reactive electricity in both directions, towards and away from the grid. The control equations of the Fractional Order Proportional Integral Derivative (FOPID) controller are presented in the following formulations:

$Q_{ref=}Q_{setpoint}t-Q_{actual}$

$e(t)=Q_{ref}$

$u(t)=K_{pe}(t)+K_i\int 0te(t)dt+K_d.d_e(t)/dt+K_{\mu D\mu e}(t)$ Eq.16

$V_{q\_ref} = V_{q\_ref}\_0+u(t)$

Where:

Q_{ref}: Reactive power reference.

$Q_{setpoint}$: Desired reactive power setpoint.

Q_{actual}: Actual reactive power.

e(t): Error signal.

u(t): Control signal.

The benefits of the PID component, Kp, Ki, and Kd.Kμ, include the FOPID fractional order derivative gain.

Dμ: Caputo fractional derivative operator of order μ.

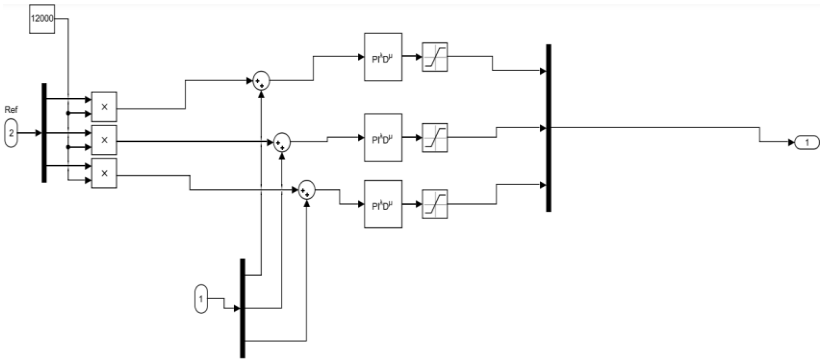

Figure 11 Fractional PID

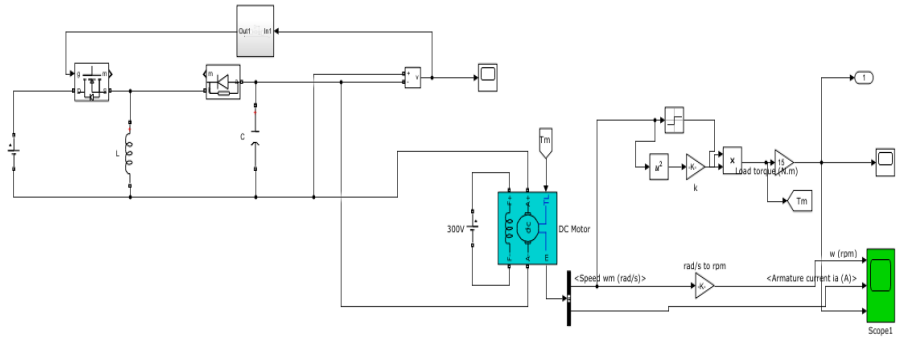

Figure 12 RSC motor subsystems

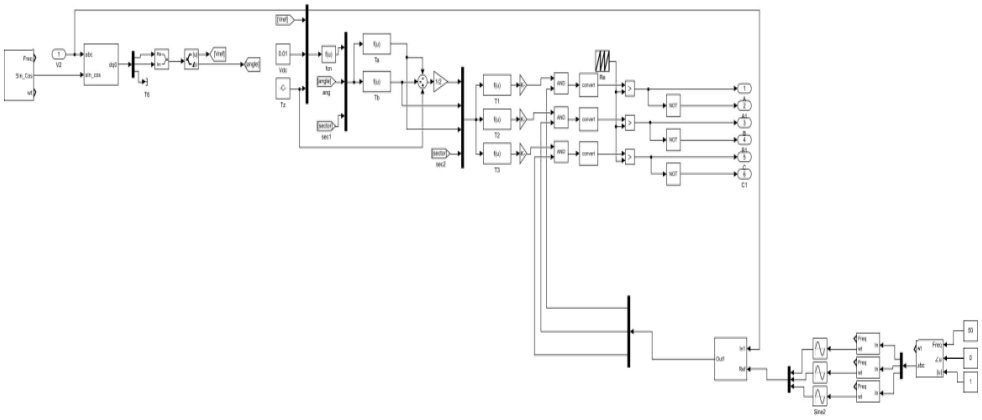

Figure 13 motor subsystems

Unity Power Factor Control in RSC: The goal of the RSC control is to regulate the rotor currents in order to attain a power factor of one, hence optimizing the extraction of energy from the wind. The equations governing the control of unity power factor can be represented as follows:

$$Iq_{r\_ref} = -X_r V_{ds}$$

$$Id_{r\_ref} = X_r V_{qs}$$

Where:

- Iq_{r_ref}: Reference q-axis rotor current.
- Id_{r_ref}: Reference d-axis rotor current.
- V_{ds} : Stator d-axis voltage.
- V_{qs}: Stator q-axis voltage.
- X_r: Rotor reactance.

International Journal of
INTELLIGENT SYSTEMS AND APPLICATIONS IN ENGINEERING
ISSN:2147-6799 www.ijisae.org Original Research Paper

5.Experimental Results

Figure 14 shows the picture of the real test bench for testing the suggested controlling solution the system consists of a 3-inch diameter pump pipe driven by a motor with a voltage of 400 volts and a capacity of 1.5 kilowatts, drawing a total current of 4.8 amps across three phases. These motor powers a pump connected to four sprinklers, each covering an area of approximately 1963.5 square meters with a 25-meter radius. The system is designed for a sprinkler irrigation setup powered by a wind turbine. However, the exact water consumption per sprinkler remains undetermined due to the absence of specific flow rate data from the pump and efficiency details of the motor and pump system.

Table 1 Parameters Detail

Component	Details
Pump Pipe Diameter	3 inches
Motor Voltage	400 volts
Motor Capacity	1.5 kilowatts (kW)
Current Drawn per Phase	1.6 amps
Total Current (Three Phases)	4.8 amps
Number of Sprinklers	4
Sprinkler Radius	25 meters
Area Covered per Sprinkler	≈ 1963.5 square meters

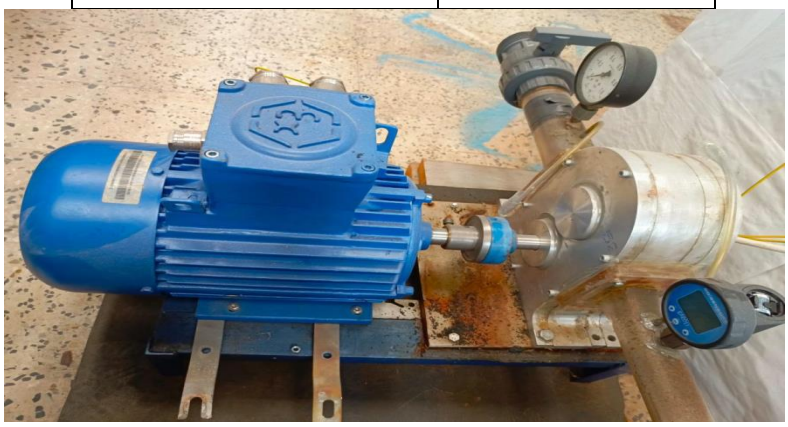

Figure 14 Experimental Motor

Sprinkler System Specifications

- **Number of Sprinklers:** 4
- **Sprinkler Radius:** 25 meters
- **Area Covered by Each Sprinkler:**

  The area covered by one sprinkler (assuming circular coverage) is calculated using the formula:
  $\text{Area}=\pi\times\text{Radius}^2$

Figure 15 Motor Design Specification

5.1 Motor Power Calculation

Motor Voltage (V): 400 volts

Frequency (f): 50 Hz

Motor Power (P): 1.5 kilowatts (kW) = 1500 watts (W)

Total Current (I): 4.8 amps (A)

Power Factor (pf): To find the power factor, we can use the formula:

$$P=\sqrt{3}\times V\times I\times pf \quad \text{Eq.18}$$

$$Pf = \frac{P}{\sqrt{3}\times V\times I}$$

Substituting the given values:

$$Pf = \frac{1500}{\sqrt{3}\times 400\times 4.8}$$

$$pf \approx \frac{1500}{33.21.12} \approx \mathbf{0.4515}$$

5.2 Total Power Supplied

The total apparent power (S) supplied to the motor can be calculated using:

$$P=\sqrt{3}\times V\times I \quad \text{Eq.19}$$

Substituting the given values:

$S=\sqrt{3}\times 400\times 4.8$

$S\approx 3321.12$ VA (Volt-Amps)

5.3 Flow Rate Estimation

To estimate the water flow rate (Q), we use the power equation for pumps, which relates the power to flow rate, head, and efficiency. The water consumption per sprinkler in this irrigation system, the system features a motor with a voltage of 400 volts and a power capacity of 1.5 kilowatts, drawing a total current of 4.8 amps across three phases. These motor drives a pump with a 3-inch diameter pipe and are part of a wind turbine-powered sprinkler irrigation system. Each of the four sprinklers in the system has a radius of 25 meters, covering an area of approximately 1963.5 square meters per sprinkler. To estimate the water flow rate from the pump, we use the motor power and typical pump efficiency. Assuming the pump operates with an

efficiency of 90% (0.7) and a typical head of 20 meters (a common value for many pumps),

$$Q= \frac{P \times \eta}{\rho \times G \times H} \quad \text{Eq.20}$$

Substitute the values

$$Q= \frac{1500 \times 0.9}{1000 \times 9.81 \times 20}$$

Calculate Q

$$Q= \frac{1350}{196200} \approx \mathbf{0.0069\ m3/s}$$

Convert to liters per second:

$$Q \approx 0.0069 \times 1000 = 6.9\ L/s$$

5.4 Water Consumption per Sprinkler

The total flow rate of 6.9 liters per second is distributed among the four sprinklers:

$$Q_{sprinkler} = \frac{6.9}{4} \approx 1.725\ L/s$$

6. Measured Results and Discussion

The simulation results validate the effectiveness of the proposed control strategy for the (RSC) and GSC in a DFIG-based wind energy system interfaced with the grid. The vector control strategy successfully decouples the d and q axes, allowing independent control of active and reactive power, thus maintaining stable and efficient power output under varying wind conditions. The system performs optimally in sub-synchronous, hyper-synchronous, and synchronous modes, demonstrating adaptability to different wind speeds. Voltage and current waveforms at the rotor and stator sides remain stable with minimal harmonic distortion, indicating effective oscillation mitigation. The DC link voltage is consistently regulated, ensuring seamless active power transfer from the rotor to the grid. Additionally, reactive power control by the GSC effectively maintains grid voltage and power quality. These results confirm the proposed strategy's ability to enhance the performance, reliability, and efficiency of grid-interfaced DFIG-based wind energy systems.

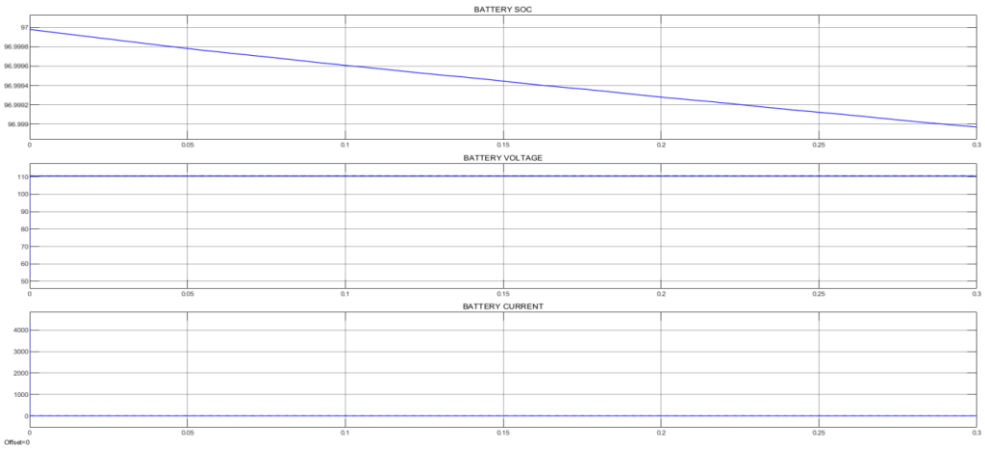

Figure 16 battery response output

Figure 17 illustrates the battery response output, highlighting the relationship between the output current, voltage, and State of Charge (SOC). In the observed scenario, the battery delivers an output current of 4000 A at a voltage of 110 V, with the SOC maintained at 97%. This high current output indicates that the battery is operating under a significant load while still maintaining a stable voltage, which reflects the battery's robust capacity and efficiency.

International Journal of
INTELLIGENT SYSTEMS AND APPLICATIONS IN ENGINEERING
ISSN:2147-6799 www.ijisae.org Original Research Paper

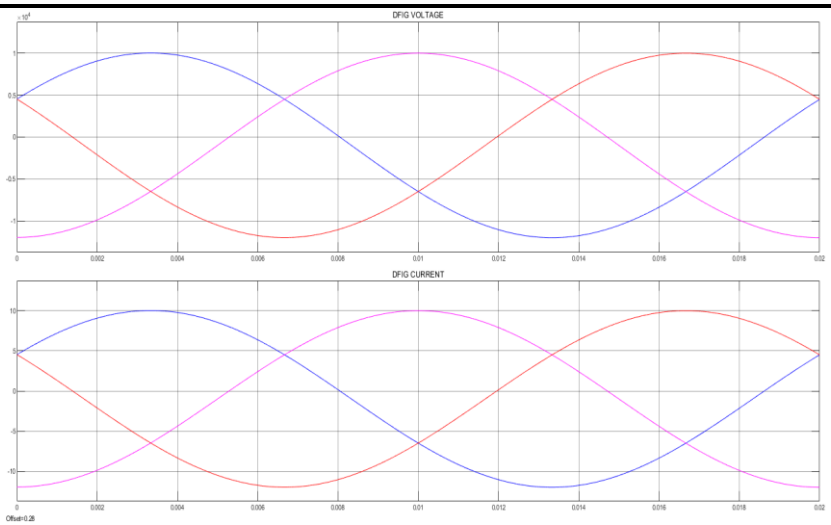

Figure 17 DFIG voltage and current

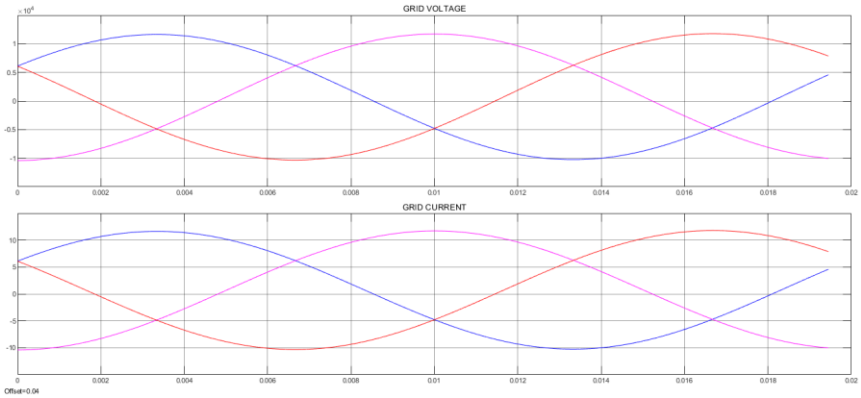

Figure 18 grid voltage and current

Figure 19 illustrates the grid current is 7 A, while the grid voltage is represented 0.7×10^4 V, which equals 7,000 V. This indicates a typical medium-voltage level in a power distribution network. The grid current of 7 A, flowing at a voltage of 7,000 V, suggests that the system is operating under a moderate load condition.

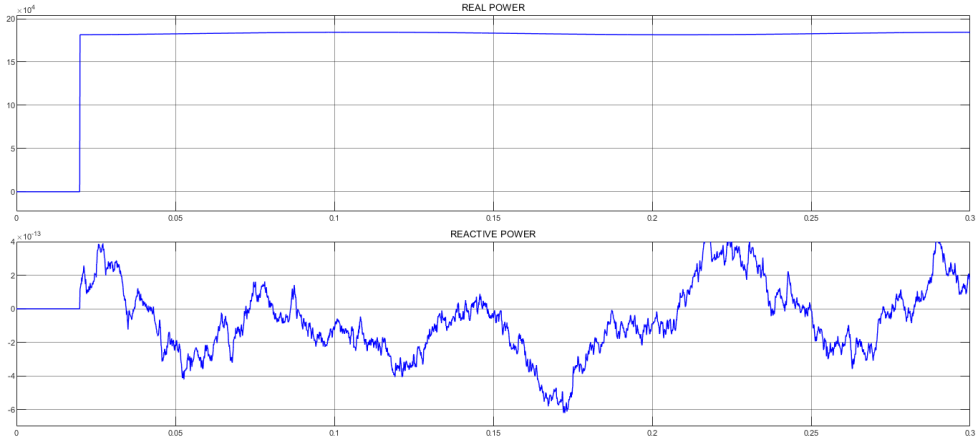

Figure 19 real and reactive power

The Figure 19 illustrating real and reactive power employs specific scaling factors on the Y-axes. The Y-axis for real power is scaled as 20×10^4 .The observed real power value of 18 on this scale

corresponds to an actual power of $18\times20\times10^4$, which equals 360,000 watts (or 360 kW). For reactive power, the Y-axis is scaled as 4×10^{-13}, The reactive power value of 4 on this scale translates to an actual reactive power of 4×10^{-13}, equating to 1.6×10^{-12} VAR.

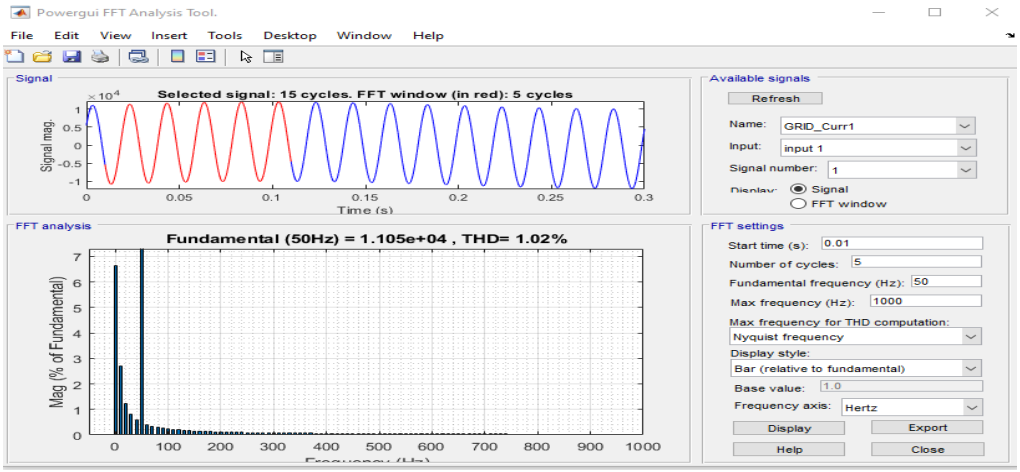

Figure 18 THD Performance

The figure 18 showing the total harmonics distortion performance the result validates the efficiency of the suggested control method for the RSC and GSC in a DFIG based wind energy system. The system show modest harmonic distortion in voltage and current waveforms, with a THD of grid current measured at 1.01%, demonstrating exceptional dependability and performance.

7. Conclusion

The proposed control strategy for the Rotor Side Converter (RSC) and Grid Side Converter (GSC) in a Doubly Fed Induction Generator (DFIG)-based wind energy system, as demonstrated through MATLAB simulations, highlights a significant advancement in managing dynamic interactions between wind turbines and the grid. The vector control strategy effectively decouples the d and q axis components, enabling precise and independent control of active and reactive power. This results in stable and efficient power output across various operational modes—synchronous, hyper-synchronous, and sub-synchronous—while adapting to changing wind conditions. The regulation of DC link voltage ensures efficient power transmission from the rotor to the grid, and the reactive power control maintains grid voltage stability and power quality. The minimal harmonic distortion in voltage and current waveforms underscores the system's reliability and performance. Overall, this control strategy enhances the adaptability, efficiency, and robustness of grid-interfaced DFIG-based wind energy systems, making it a promising solution for integrating renewable energy into the power grid.Similarly, in the irrigation system driven by a 1.5-kilowatt motor operating at 400 volts and drawing a total current of 4.8 amps, the pump connected through a 3-inch diameter pipe delivers water to four sprinklers. Assuming a pump efficiency of 90% and a head of 20 meters, the pump provides a total flow rate of approximately 6.9 liters per second. When distributed among the four sprinklers, each sprinkler consumes about 1.725 liters of water per second. This calculation highlights the importance of pump efficiency in optimizing water delivery. A higher pump efficiency ensures a better flow rate, allowing each sprinkler to effectively cover its designated area of about 1963.5 square meters with a 25-meter radius. Efficient water distribution is crucial for maintaining the effectiveness of the irrigation system, supporting the health of the vegetation being irrigated, and optimizing resource usage.

References

1. IRENA. Renewable Energy Policies in a Time of Transition; IRENA: Abu Dhabi, UAE, 2018; Volume 4, pp. 62–64.
2. WWEA. Wind Power Capacity Worldwide Reaches 597 GW, 50.1 GW. 2018. Available online: https: //wwindea.org/information-2/information/ (accessed on 16 February 2020)
3. H. Polinder, J.A. Ferreira, B. B. Jensen, A. B. Abrahamsen, K. Atallah, and R. A. McMahon, “Trends in wind turbine generator systems,” IEE J. Emerg. Sel. Topics on Power Electron., vol. 1, no. 3, pp. 174-185, Sep. 2013.
4. G. Abad, G. Iwanski, J. López, L. Marroyo, and M. Rodríguez, “Doubly Fed Induction Machine: Modeling and Control for Wind Energy Generation Applications”. Hoboken, NJ, USA: Wiley, 2011.
5. R. Pena, J. C. Clare and G. M. Asher, “Doubly fed induction generator using back-to-back PWM converters and its application to variable speed windenergy generation,” IEE Proc.-Elect. on Power Appl., vol. 143, no. 3, pp. 231-241, May 1996.

6. L. Xu and P. Cartwright, “Direct active and reactive power control of DFIG for wind energy generation,” IEEE Trans. On Energy Convers., vol. 21, no. 3, pp. 750-758, Sep. 2006.

7. W. Qiao, W. Zhou, J. M. Aller and R. G. Harley, “Wind speed estimation based sensorless output maximization control for a wind turbine driving a DFIG,” IEEE Trans. on Power Electron., vol. 23, no. 3, pp. 1156-1169, May 2008.

8. H. Nian, Y. Song, P. Zhou and Y. He, “Improved direct power control of a wind turbine driven doubly fed induction generator during transient grid voltage unbalance,” IEEE Trans. on Energy Convers., vol. 26, no. 3, pp. 976-986, Sept. 2011.

9. H. Polinder, J. A. Ferreira, B. B. Jensen, A. B. Abrahamsen, K. Atallah, and R. A. McMahon, “Trends in wind turbine generator systems,” IEEE J. Emering. Select. Topics on Power Electron, vol. 1, no. 3, pp. 174-185, Sept. 2013.

10. D. Zhi, L. Xu and B. W. Williams, “Improved direct power control of grid-connected DC/AC converters,” IEEE Trans. on Power Electron., vol. 24, no. 5, pp. 1280-1292, May 2009.

11. S. Vazquez, J. A. Sanchez, J. M. Carrasco, J. I. Leon and E. Galvan,“A model-based direct power control for three-phase power converters,” IEEE Trans. on Ind. Electron., vol. 55, no. 4, pp. 1647-1657, Apr. 2008.

12. D. Zhi and L. Xu, “Direct power control of DFIG with constant switching frequency and improved transient performance,” IEEE Trans. on Energy Convers. vol. 22, no. 1, pp. 110-118, Mar. 2007.

13. P. Zhou, Y. He and D. Sun, “Improved direct power Ghulam Sarwar Kaloi, Jie Wang and Mazhar Hussain Baloch http://www.jeet.or.kr │control of a DFIG based wind turbine during network unbalance,” IEEE on Trans. Power Electron., vol. 24, no. 11, pp. 2465-2474, Nov. 2009.

14. D. Zhi, L. Xu and B. W. Williams, “Model-based predictive direct power control of doubly fed induction generators,” IEEE Trans. on Power Electron., vol. 25, no. 2, pp. 341-351, Feb. 2010

15. N. Amiri, S. M. Madani, T. A. Lipo, and H. A. Zarchi, “An improved direct decoupled power control of doubly fed induction machine without rotor position sensor and with robustness to parameter variation,” IEEE Trans. on Energy Convers., vol. 27, no. 4, pp. 873-884, Dec. 2012.

16. J. Hu, H. Nian, B. Hu, Y. He and Z. Q. Zhu, “Direct active and reactive power regulation of DFIG using sliding-mode control approach,” IEEE Trans. on Energy Convers., vol. 25, no. 4, pp. 1028-1039, Dec. 2010.

17. Balogun, O. Ojo and F. Okafor, “Decoupled direct control of natural and power variables of doubly fed induction generator for extended wind speed range using feedback linearization,” IEEE J. Emerg. Sel. Topics on Power Electron., vol. 1, no. 4, pp. 226-237, Dec. 2013.

18. P. Krause, O. Wasynczuk, S. Sudhoff and I. P. E. Society, Analysis of Electric Machinery and Drive Systems. Piscataway, NJ: IEEE, 2002.

19. R. Esmaeil, A.Tabesh and M. Ebrahimi, "Dynamic model and control of DFIG wind energy systems based on power transfer matrix." IEEE Trans. on Power Delivery, vol. 27,no. 3,pp 1485-1493, July. 2012.

20. Mohammad Nasir Uddin;Md. Shamsul Arifin;Nima Rezaei (2023) “A Novel Neuro-Fuzzy Based Direct Power Control of a DFIG Based Wind Farm Incorporated With Distance Protection Scheme and LVRT Capability” IEEE Transactions on Industry Applications 2023 , Volume: 59, Issue: 5 ,Journal

21. Souvik Das;Bhim Singh(2023)‘Normalized Maximum Correntropy Criterion Based Ripple Mitigation Strategy for Wind–Solar Hybrid Generation System Under Nonideal Grid Conditions “IEEE Transactions on Power Electronics 2023 ,Volume: 38, Issue: 1 ,

22. Alberto Berrueta;Javier Sacristán;Jesús López;José Luis Rodríguez;Alfredo Ursúa;Pablo Sanchis (2023) “Inclusion of a Supercapacitor Energy Storage System in DFIG and Full-Converter PMSG Wind Turbines for Inertia Emulation” IEEE Transactions on Industry Applications 2023 , Volume: 59, Issue: 3

23. Subodh Kumar Mohanty;Paresh Kumar Nayak;Pallav Kumar Bera;Hassan Haes Alhelou(2024)“An Enhanced Protective Relaying Scheme for TCSC Compensated Line Connecting DFIG-Based Wind Farm” IEEE Transactions on Industrial Informatics 2024 , Volume: 20, Issue: 3

24. Md. Shamsul Arifin;Mohammad Nasir Uddin;Wilson Wang(2023) “Neuro-Fuzzy Adaptive Direct Torque and Flux Control of a Grid-Connected DFIG-WECS With Improved Dynamic Performance” IEEE Transactions on Industry Applications2023 ,Volume: 59, Issue: 6 |

25. Mohammed Alqahtani;Zhixin Miao;Lingling Fan(2023) “Harmonic Analysis of Type-3 Wind Turbines Subject to Grid Unbalance” IEEE Open Access Journal of Power and Energy2023 Volume: 10

26. S. Chen, N. Cheung, K. Wong and J. Wu, “Integral variable structure direct torque control of doubly fed induction generator,” IET Renew. on Power Gen., vol. 5, no. 1, pp. 18-25, 2011.

27. M. K. Bourdoulis and A.T. Alexandridis, "Direct

power control of DFIG wind systems based on nonlinear modeling and analysis," IEEE J. Emerg. Sel. Topics on Power Electronics, vol. 2, no. 4, pp. 764-775, Dec. 2014.

28. T. Ahmadreza and R. Iravani. "Multivariable dynamic model and robust control of a voltagesource converter for power system applications," IEEE Trans. on Power Delivery, vol. 24, no.1, pp. 462-471. Jan. 2009.
29. R. Mohsen and M. Parniani. "Transient performance improvement of wind turbines with doubly fed induction generators using nonlinear control strategy," IEEE Trans. on Energy Conversion, vol. 25, no .2, pp. 514-525. June. 2010.
30. Boukhezzara, L. Lupua, H. Siguerdidjanea, M. Handb: Multivariable control strategy for variable speed, variable pitch wind turbines, Renewable Energy, Vol. 32, Issue 8, pp, 1273-1287, 2007.
31. H. Camblonga, I. Martinez de Alegriab, M. Rodriguezc and G. Abadc: Experimental evaluation of wind turbines maximum power point tracking controllers, Energy Conversion and Management, Vol. 47, issues 18-19 , pp. 2846- 2858, 2006
32. Rekioua, D.; Matagne, E. Optimization of Photovoltaic Power Systems Modelization, Simulation and Control; Bentham Science Publishers: Sharjah, United Arab Emirates, 2012.
33. Dufo-López, R.; Lujano-Rojas, J.M.; Bernal-Agustín, J.L. Comparison of different lead–acid battery lifetime prediction models for use in simulation of stand-alone photovoltaic systems. Appl. Energy 2014, 115, 242–253.
34. Sauer, D.U.; Wenzl, H. Comparison of different approaches for lifetime prediction of electrochemical systems Using lead–acid batteries as example. J. Power Sources 2008, 176, 534–546.